



## Energy Absorption Study of Aluminium Profiles with Variety of Filling Configurations

Paweł BOGUSZ, Michał STANKIEWICZ, Grzegorz SŁAWIŃSKI

*Department of Mechanics and Applied Computer Science  
Faculty of Mechanical Engineering  
Military University of Technology*

Gen. S. Kaliskiego 2, 00-908 Warszawa, Poland  
e-mail: {pawel.bogusz, michal.stankiewicz, grzegorz.slawinski}@wat.edu.pl

The subject of this paper is research of thin-walled aluminium profiles filled with different materials and subjected to dynamic load. The aim of this study was to determine the crashworthiness capabilities of the tested elements. Such structures can be used as elements minimalising the effects of blast wave load on military vehicles and occupants carried thereon. The blast wave generated during the explosion of explosives, especially improvised explosive devices (IED), under or near a combat vehicle poses a deadly threat to the crew and passengers inside the vehicle. The idea of installing crashworthy structures in a vehicle seat to protect the crew and passengers is not new. It was found useful in aviation, automotive or railway industry. In this paper, circular aluminium profiles of an external diameter of 50 mm and thickness of 2 mm were investigated. They were filled with three kinds of materials: cork, foamed aluminium of low density and foamed aluminium of high density. The dynamic tests were performed on a spring hammer apparatus. The energy absorbing structures and materials used to fill the aluminium profiles were examined separately in static compression tests. The characteristics of force-displacement response of the investigated structures were determined, compared and analysed. The energy absorbing characteristic parameters were obtained and discussed to determine the best option.

**Key words:** energy absorbing tests, energy absorbing structures, aluminium structures, foamed materials, cork, experimental research.

### 1. INTRODUCTION

Foam-filled structures are widely studied in many papers. An increase of the crushing force in these structures is obtained from the direct compressive strength of the foam and from the interaction between the foam and the wall column [3, 6, 14, 16].

Paper [14] presents comprehensive experimental and numerical studies of the crush behaviour of aluminium foam-filled sections undergoing axial compressive loading. Non-linear dynamic finite element analyses were carried out to simulate

quasi-static test conditions, which were found to be in good agreement with the experimental results. The authors found that the increase in mean crushing force of a filled column shows a linear dependence on the foam compressive resistance and a cross-sectional area of the column.

In [7], braided glass-fibre/epoxy circular tubes with polymer foam cores were loaded in tension and in compression, and the energy of deformation was measured. Theoretical models of tube deformation were developed to predict the energy absorption as a function of tube wall strength, the ratio of tube wall thickness to the tube diameter, and the density of the foam. The energy per unit mass and energy per unit volume were optimised with respect to the relative density and geometry. Foam-filled braided circular tubes were found to be effective in case of energy absorbing characteristics, due to a combination of energy absorption by the polymeric foam core and by the glass/epoxy braided tube.

The effect of low-density metal filler, such as aluminium foam or honeycomb, on the bending collapse resistance of thin-walled prismatic columns was studied and presented in [16]. A combination of analytical and numerical results was used to predict the initial and post-collapse response of both empty and filled columns. The low-density metal core retarded sectional collapse of the thin-wall column, and increased bending resistance for the same rotation angle. Numerical simulations showed that, in terms of achieving the highest energy absorption to weight ratio, columns with aluminium honeycomb or foam core were preferable for thickening the column wall. Additionally, the presence of adhesive improved significantly the specific energy absorption.

A blast wave generated during the explosion of explosives under or near a combat vehicle is very dangerous to the occupants of a combat vehicle. The most common threats in modern conflicts are improvised explosive devices (IED), due to their relatively easy construction. Much effort is put to reduce the impact pulse to the minimum, and thereby to increase chances of survivability and to maximally reduce injuries resulting from the shock wave of explosion. The small energy-absorbing structures installed in the construction of seats can help achieve that objective. The crashworthy structures protecting the crew and passengers were found useful in aviation, automotive or railway industry, especially in military applications.

Floors of helicopters use energy-absorbing structures to protect the crew and passengers from the effects of emergency landing. The impact energy of emergency landing is converted into breaking landing gear, as well as destroying seats and a lower structure of the helicopter fuselage along with the crashworthy elements [19]. Nowadays, sandwich structures, aluminium, foamed materials, also combined with each other, are widely used as energy-absorbing materials. A honeycomb insert made of aluminium was used to fill aluminium fins underside the fuselage of Augusta helicopter [12].

In [8], the long-term engineering experience at Cranfield Impact Centre Ltd. in the field of crashworthiness of thin-walled beams and joints in vehicle structures was summarised. It covers, among others, such problems as: complex approach to crashworthiness design and analysis of beams and joints treated separately from complete structures, deep bending collapse of beams and joints from the static and dynamic testing, and analytical prediction perspectives.

Paper [2] reviews the common shapes of collapsible energy absorbers and different deformation modes of the most common structures. Common shapes include circular tubes, square tubes, frusta, struts, honeycombs, and sandwich plates. Common modes of deformation for circular tubes include axial crushing, lateral indentation, lateral flattening, inversion and splitting.

Energy absorber components in the form of aluminium profiles filled with foamed materials are also used in railway construction of energy absorbing crumple zones. The extensive literature [10, 11, 13, 18] presents the results of both experimental and numerical simulation research on the impact absorbers used in the construction of wagon crumple zones (Fig. 1).

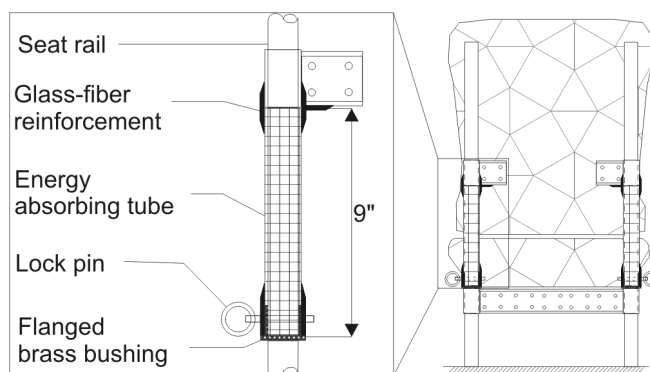


FIG. 1. Crush tube energy absorbing concept in an agricultural aircraft seat (based on Fig. 3 [9]).

In [9], a task was initiated to improve the energy absorption capability of an agricultural aircraft seat through cost-effective redesigning, while keeping a seat-weight increase to a minimum. Only vertical crash scenarios, which required the energy absorbing system to protect the seat occupant in a range of crash speeds up to 31 ft/sec, were considered. The authors assumed that the forward and/or side crash accelerations could be attenuated with the aid of airbags. A conceptual design as well as fabrication and testing (static and dynamic) of energy absorbers were carried out. Next, testing of the actual modified seat system with a dummy occupant was performed.

One of the two concepts evaluated in the above paper was a crush tube energy absorbing concept presented in Fig. 1. In this solution, the impact energy

is absorbed through the plastic deformation of a 9" long aluminium tube during the compressive stroke of the seat. The crush tubes were integrated into the seat system with glass reinforced fabric to couple one aluminium tube to the bottom of each top bracket.

Full scale tests were performed. The tests results indicated that occupant loads were attenuated successfully to survivable levels. The occupant maximum lumbar load was reduced from 1936 lb., which resulted from a velocity at impact of 25.7 ft/sec, to 1500 lb resulting from a 32.5 ft/sec test [9].

In [17], numerical studies on the design of the seat intended for a combat vehicle were presented. An aluminium tube was integrated with a frame of the seat (Fig. 2). The use of an energy absorbing seat in conjunction with vehicle armour plating was intended to improve occupant survivability during an explosive blast. The dynamic axial crushing of aluminium tubes constituted a principal energy absorption mechanism to reduce a blast pulse transmitted to the occupant. The injury mechanisms of both vehicle-occupant contact interfaces were simulated, namely, a vehicle seat upon the occupant's torso and a vehicle floor upon the occupant's feet. Data such as a hip and knee moment, femoral force, and foot acceleration were collected from the numerical dummy used to simulate the occupant's response. This data was then compared to injury threshold values from various references to assess survivability [17].

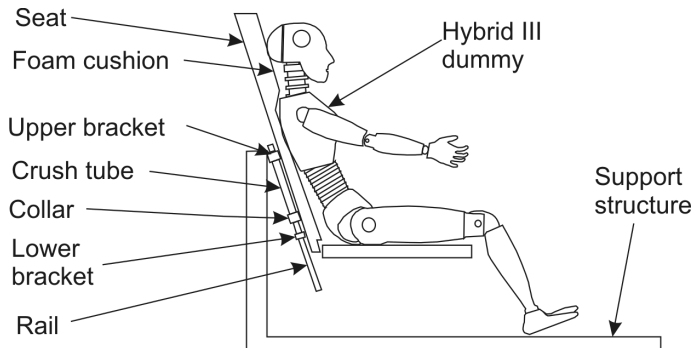


FIG. 2. Structure of energy absorbing seat of combat vehicle (based on Fig. 1 [17]).

In the authors' opinion, the evaluated energy absorbing seat design proved to be effective in occupant survivability during a vertical drop test and mine blast scenarios. The numerical results of the simulations proved that crushing of aluminium tubes provides controlled, acceptable means of reducing deceleration pulses to survivable values. The use of a contoured foam cushion and contoured headrest additionally helped minimising a gap between the body and the seat decreasing the peak deceleration pulse at the occupant's body.

Concluding, the use of the HYBRID III dummy to simulate occupant response during mine blast testing was satisfactorily validated by the simulation results in good agreement with the experimental data [17].

In [1], a mine blast resistant kit, developed and designed to enhance the survivability of the crew of military trucks, was studied. The kit included an energy-absorbing (EA) seat - a focus of [1]. A full-scale demonstration mine blast of a 5-ton truck was conducted using the full protection kit and included two anthropomorphic dummies to represent the passenger and driver. The passenger manikin was seated in the EA seat, whereas the driver manikin was seated in a standard seat. The results show the standard seat produced lumbar (lower back) spine compression of 2159 lbs, a value that exceeds the 1500 lb threshold generally used in a spinal injury assessment. On the other hand, the EA prototype seat limited the compression of the lower spine to about 1329 lbs, a value which is below injury thresholds.

It was concluded that the mine protection kit reduced upward truck accelerations transmitted to the truck occupants and eliminated head contact injuries, and the EA seat reduced lumbar spine compressive forces by 38% to a level below a tolerance threshold [1].

## 2. RESEARCH METHODOLOGY

The above presented examples clearly show that aluminium structures can be very effective in mitigating the negative impacts of crush and even blast wave pulses, and can attenuate acceleration impact transmitted to the crew and passengers of a vehicle to the survivability level.

In this research, circular aluminium profiles, made of 6060-T66 (known as PA38 in Poland) alloy, with different filling configurations were investigated. Static and dynamic tests were performed. Dynamic tests were thoroughly analysed as typical energy-absorbing structures are designed to work in dynamic conditions.

The specimens were made on the basis of aluminium profiles, cut directly from a pipe with an outer diameter of 50 mm, wall thickness of 2 mm and height of 100 mm. Characteristic physical properties of the specimens are presented in Table 1.

The aluminium profiles were examined in four filling configurations presented in Fig. 3. First configuration was the empty tube, i.e., without any filling – Fig. 3a. The tube average mass was equal to 80.4 g. The second variant was a tube filled with NL25 cork with density of  $0.25 \text{ g/cm}^3$ , which was named Cork\_NL25 – Fig. 3b. The total average mass of this specimen was equal to 124.0 g. Tubes filled with aluminium Alporas foam with density of  $0.36 \text{ g/cm}^3$ , and with the total average mass of 138.0 g, were used as the third configura-

**Table 1.** Physical properties of the tubes and cores.

Name	Tube material	Tube average mass [g]	Tube outer/inner diameter/thickness [mm]	Volume total/core [cm <sup>3</sup> ]	Core material	Nominal core density [g/cm <sup>3</sup> ]	Total average mass [g]	Core average mass [g]
Empty tube	Aluminium 6060 T66 (PA38)	80.4	50/46/2	196.35/166.19	none	–	80.4	–
Cork_NL25					Cork N25	0.25	124.0	43.6
Foam_A					Aluminium foam	0.35	138.0	57.6
Foam_B					Aluminium foam	0.51	164.6	84.2

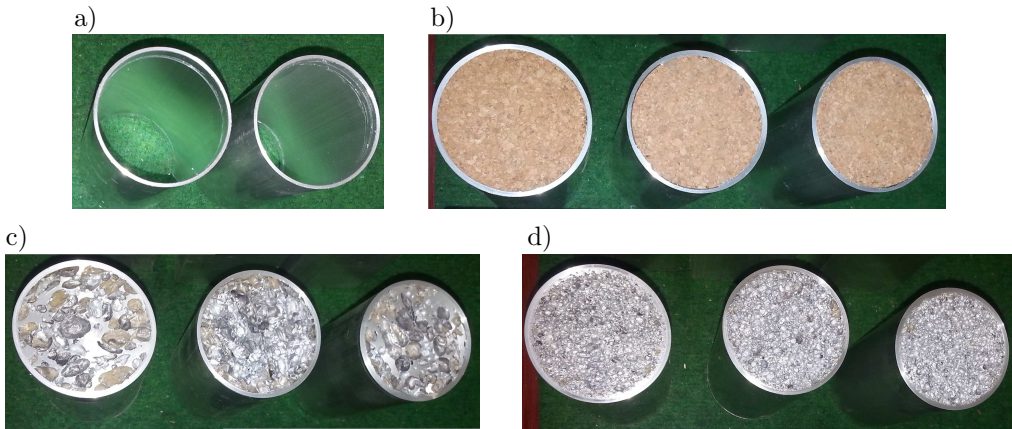


FIG. 3. Samples of aluminium profiles with the examined configurations: a) without filling, b) filled with NL25 cork, c) filled with aluminium foam with density of  $0.36 \text{ g/cm}^3$ , d) filled with aluminium foam with density of  $0.51 \text{ g/cm}^3$ .

tion. The samples filled with low density foam are presented in Fig. 3c and are named Foam\_A in the presented graphs. The fourth configuration is a tube filled with the same aluminium Alporas foam but in this case with higher density of  $0.51 \text{ g/cm}^3$ , and the average mass of 164.6 g. This sample was named as Foam\_B on the graphs – Fig. 3d.

The cores were cut to fit the inner diameter of the cylinders using water jet cutting and next they were placed under some pressure inside the tubes, without using any glue. The inserts height is limited, as they are sold in sheets with predetermined height, which is typically about a few centimetres. Foam\_A and Foam\_B have a 26 mm height each and the Cork\_NL25 is 50 mm high. Four pieces composed of either aluminium foams or two cork parts were put inside each of the filled tubes. Excesses of the cores were cut or milled.

Three samples were tested in dynamic conditions for each considered configuration. The empty configuration was tested with two samples. Additionally, dynamic results are compared in the presented compression graphs with an example sample compressed under static load. The representative sample data is marked with a dotted line. Dimensions and preparation process of the samples loaded statically are the same as in the case of the specimens investigated with dynamic load.

The dynamic tests were performed using the spring hammer testing apparatus shown in Fig. 4. Most of the impact energy results from the compression of the hammer springs. The impact velocity of the hammer beater was equal to 6.7 m/s and the dropping weight was equal to 95.6 kg. The impact energy was then equal to 2.12 kJ.



FIG. 4. Spring hammer testing apparatus used the for dynamic impact tests.

The crushing force was measured through direct measurement with a piezoelectric sensor force PCB Piezotronic 207C, in the range of  $\pm 450$  kN, and then scaled with a scale factor of the sensor provided by the manufacturer. The sensor was mounted on the round measurement table installed on the base of the hammer. The measurement of displacement of the hammer beam was carried out with a laser triangulation sensor Keyence. Data was acquired by coupling a high-speed data acquisition card to a computer. Sampling frequency was equal to 50 kHz.

Standard static compression tests were performed on a universal hydraulic machine Instron 8802. Structures of all types of configurations, with the same dimensions and preparation procedure, were examined. A constant test speed was equal to 50 mm/s. The data logging system was running at a constant rate of 1 kHz.

Additionally, the rectangular specimens of filling materials: Foam\_A, Foam\_B and Cork\_Nl25 with dimensions of  $50 \times 50$  mm were tested. The cork material had double the height of the other two insert materials. Foam\_A and Foam\_B had 26 mm height each and the Cork\_Nl25 – 50 mm. A constant test speed and a sampling rate were set the same as in the case of static compression test of the structures.

Based on the obtained data, compression graphs of force in the function of specimen shortening were obtained for all investigated structure versions. For each core variant, dynamic curves were compared with the exemplary curve from the static loading test. Characteristic energy absorbing parameters were evaluated and analysed.

### 3. RESEARCH RESULTS

Next, the analysis of energy absorbing capabilities of the investigated structures was carried out. The results of the dynamic compression tests and calculated data are presented in Tables 2 and 3.

Peak of crushing force (PCF) corresponds to maximum force at the beginning of the crush. Mean crushing force (MCF) is an average force during a plateau.

**Table 2.** Test results for aluminium profiles with different configurations of fillings.

Name	Filling	Maximum compression [mm]	Peak crushing force [kN]	Mean crushing force [kN]	Crushing load efficiency	Useful stroke* [mm]	Stroke efficiency*
Spec.2	Empty tube	44.4	75.6	28.5	0.38	–	–
Spec.3		46.6	75.7	28.8	0.38	–	–
<b>Average:</b>		<b>45.5</b>	<b>75.7</b>	<b>28.7</b>	<b>0.38</b>	<b>74.4</b>	<b>0.74</b>
Spec.1	Cork_NL25	41.0	77.0	33.6	0.44	–	–
Spec.2		41.9	77.8	33.8	0.43	–	–
Spec.3		41.8	74.7	34.4	0.46	–	–
<b>Average:</b>		<b>41.6</b>	<b>76.5</b>	<b>33.9</b>	<b>0.44</b>	<b>64.6</b>	<b>0.65</b>
Spec.1	Foam_A	39.6	75.3	30.6	0.41	–	–
Spec.2		40.7	74.6	32.6	0.44	–	–
Spec.3		40.3	75.5	34.3	0.45	–	–
<b>Average:</b>		<b>40.2</b>	<b>75.1</b>	<b>32.5</b>	<b>0.43</b>	<b>64.3</b>	<b>0.64</b>
Spec.1	Foam_B	31.7	83.6	49.2	0.59	–	–
Spec.2		32.8	85.0	47.2	0.56	–	–
Spec.3		33.2	84.6	46.4	0.55	–	–
<b>Average:</b>		<b>32.6</b>	<b>84.4</b>	<b>47.6</b>	<b>0.56</b>	<b>58.6</b>	<b>0.59</b>

\* – based on the static tests

**Table 3.** Energy absorbing properties of aluminium profiles with different configurations of fillings.

Name	Filling	Crashed mass [g]	Crashed volume [cm <sup>3</sup> ]	Absorbed energy (EA) [kJ]	Specific absorbed energy [J/g]	Energy per unit volume [J/cm <sup>3</sup> ]	Volume structural efficiency
Spec.2	Empty tube	35.7	87.2	1.44	40.4	16.5	
Spec.3		37.4	91.4	1.48	39.6	16.2	
<b>Average:</b>		<b>36.6</b>	<b>89.3</b>	<b>1.46</b>	<b>40.0</b>	<b>16.4</b>	
Spec.1	Cork_NL25	50.9	80.6	1.51	29.7	18.7	1.14
Spec.2		52.0	82.3	1.54	29.7	18.7	1.14
Spec.3		51.8	82.0	1.51	29.1	18.4	1.12
<b>Average:</b>		<b>51.6</b>	<b>81.6</b>	<b>1.52</b>	<b>29.5</b>	<b>18.6</b>	<b>1.14</b>
Spec.1	Foam_A	54.6	77.8	1.49	27.3	19.2	1.17
Spec.2		56.1	79.9	1.47	26.2	18.4	1.13
Spec.3		55.7	79.2	1.50	26.9	18.9	1.16
<b>Average:</b>		<b>55.5</b>	<b>78.9</b>	<b>1.49</b>	<b>26.8</b>	<b>18.9</b>	<b>1.15</b>
Spec.1	Foam_B	52.2	62.2	1.65	31.7	26.6	1.62
Spec.2		54.0	64.4	1.68	31.2	26.2	1.60
Spec.3		54.7	65.2	1.65	30.1	25.2	1.54
<b>Average:</b>		<b>53.6</b>	<b>63.9</b>	<b>1.66</b>	<b>31.0</b>	<b>26.0</b>	<b>1.59</b>

The crush force efficiency, defined as the ratio of the average and maximum force, is a useful measure of the uniformity of collapse load.

A length of the plateau period measured from the beginning of the test to the rapid force increase at the end of the curve is described as a useful stroke (US). It corresponds to maximum shortening of a specimen, where total efficiency (TE) achieves its maximum value and begins to drop quickly due to very fast increase of maximum force. TE parameter is defined as the ratio of the actual absorbed energy (EA) to the product of actual maximum force and total specimen height [4]. UT was obtained based on the static tests of the specimens, due to insufficient impact energy of the drop hammer. Shortenings of the specimens during the dynamic load did not reach the onset of the densification displacement. Figure 5 compares the graphs of static compression tests for specimens of each variant.

Stroke efficiency (SE), which is the ratio of the US to the initial length of the tube, was also calculated. Both crush force efficiency and stroke efficiency should be as close to unity as possible for the ideal energy absorber [7].

Table 3 presents additional energy absorbing properties of the investigated structures. Based on the total mass and volume of the specimens, as well as

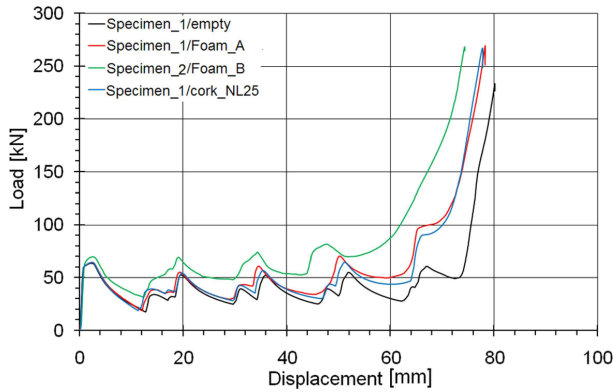


FIG. 5. Comparison of static compression results for evaluating filling configurations.

their shortenings and core mass and volume values, masses and volumes of their compressed parts were calculated.

Finally, absorbed energy (EA) as a field under the force-shortening curve was obtained. The obtained value was divided, first, by the mass of the crushed part of the specimen and, second, by the volume of the crushed part of the specimen. As a result, the specific absorbed energy (SEA) and the energy per unit volume (EA/V ratio) were obtained.

Volume structural efficiency is one of the methods for measuring the efficiency of the structure modification. It was calculated as the ratio of the energy per unit volume of the modified structure to the corresponding value of an unmodified structure, and it is presented in the last column on the right-hand side of Table 3.

In Fig. 6, the force-displacement graphs for the empty aluminium profiles are presented. Two samples were investigated in this manner. Their results are

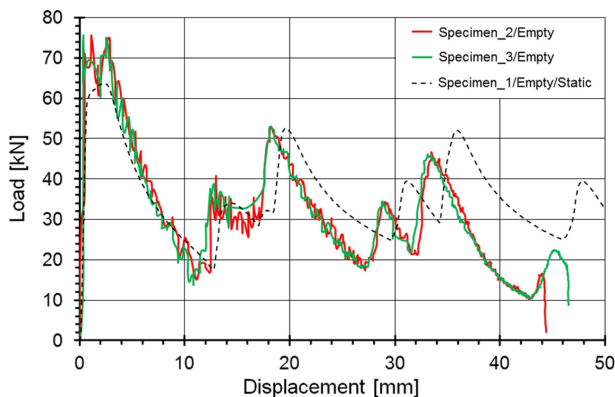


FIG. 6. Dynamic compression results for empty specimens compared with the static test results (dotted line).

similar. The maximum PCF obtained at the beginning of the impact is equal to 75.7 kN on average, whereas the average MCF is equal to 28.7 kN (Table 2). Crushing load efficiency is equal to 0.38. The average displacement is about 45.5 mm and the stroke efficiency, measured based on the static experimental tests (Fig. 5), is about 0.74. SAE is equal to about 40 kJ/kg. These are the basic parameters of energy absorbing capabilities to be used for comparison with other modified structures. The static test curve of the empty specimen from Fig. 5 is presented as a dotted line (Fig. 6) for comparison with the dynamic tests of the other specimens.

In Fig. 7, samples of a circular aluminium profile without any filling, after dynamic compression are presented. Three foldings of the profile in each specimen are clearly visible. Empty cylinders collapse in axisymmetric buckling mode. The graphs of the force are saw-like shaped. Each “tooth” corresponds to the folding of the profile (Fig. 6).



FIG. 7. Samples of circular aluminium profile without filling, after the dynamic compression.

Figure 8 presents the dynamic compression results for the Cork\_NL25-filled specimens. The shape of the force curve is similar to that of the empty profiles.

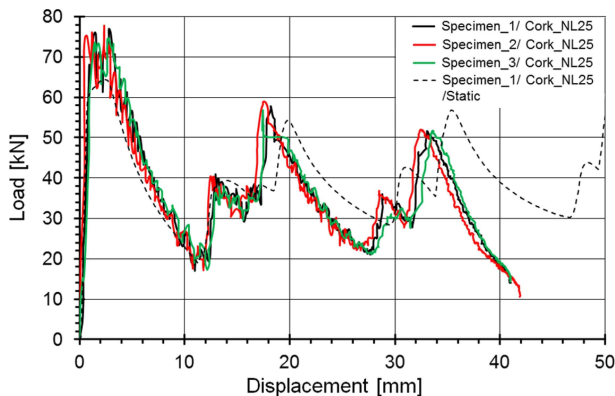


FIG. 8. Dynamic compression results for specimens filled with Cork\_NL25.

The samples after the dynamic compression testing are shown in Fig. 9. In this scenario, a folding of the metal is also present. The cork filling did not influence the maximum average force, which is similar to that observed in the empty specimens. However, MCF is slightly higher – 33.9 kN. Due to this higher MCF, the crash force efficiency increased to 0.44 and compression distance was reduced to 41.6 mm as the impact energy is limited (Table 2 and 3). Additionally, Fig. 8 shows a dotted curve representing the curve from the Cork\_NL25 static test shown in Fig. 5. This is done to compare it with the dynamic compression results of the same specimen.



FIG. 9. Samples of circular aluminium profile filled with Cork\_NL25, after the dynamic compression.

Cork material worked during the crush mainly in its elastic range, thus the cork filling returned almost to its initial height after the test. Although plastic deformation also occurred, it did not produce a significant impact on the overall cork deformation. The heights of the cork inserts measured after the tests were equal to: 95 mm for specimen\_1, 92 mm for specimen\_2, and 93 mm for specimen\_3, and on average: 93.3 mm. Additional mass of the filler significantly decreased the SAE parameter, which is equal to about 30 kJ/kg.

In Fig. 10, the static compression result and three dynamic compression results for the scenario of Foam\_A insert are presented. The graphs of force are saw-like shaped as in the case of the previous configurations. Figure 11 shows the specimens after the dynamic crush. Cylinders were crushed in axisymmetric buckling mode, while foam core was crushed plastically in a diamond buckling mode. MCF level is similar to that of a cork-filled configuration. Low density foamed metal did not influence the results as compared to the unfilled profiles. PCF and maximum compression are at the similar level as in the case of the cork filling (Table 2). Useful stroke and stroke efficiency are on the similar level in comparison to Cork\_NL25.

The data for three specimen configurations with higher density aluminium foam insert (Foam\_B) is presented in Fig. 12. The PCF parameter increased

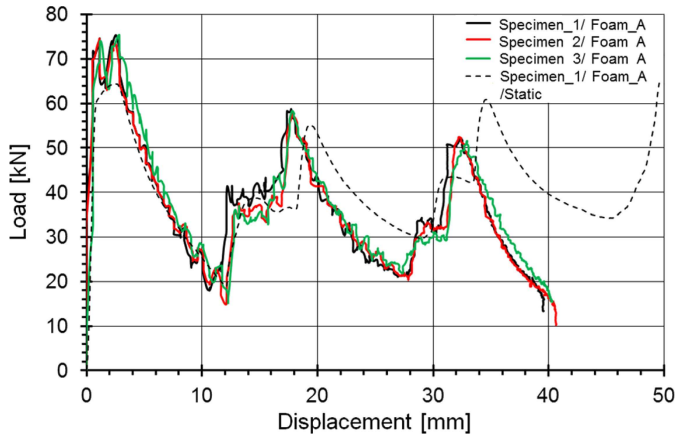


FIG. 10. Dynamic compression results for specimens filled with Foam\_A.



FIG. 11. Samples of circular aluminium profile filled with low density aluminium foam, after the dynamic compression.

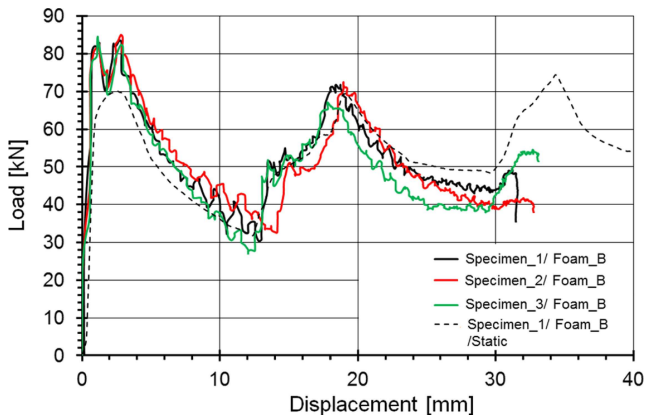


FIG. 12. Dynamic compression results for specimens filled with Foam\_B.

significantly. All three specimens were crushed with the initial maximum force of more than 84 kN. MCF was equal to 47.6 kN, which caused an increase in

load efficiency to 0.56. Due to a higher average force, a compression distance was significantly shorter and equal to about 32.6 mm on average. Thus, only two foldings of the circular profiles occurred (Fig. 13). Crushing modes of the tube and the aluminium foam insert were identical as in the case of Foam\_A. SAE of the Foam\_B structure was also better than for other filled configurations. Useful stroke and stroke efficiency were significantly smaller than in other studied specimen configurations.



FIG. 13. Samples of circular aluminium profile filled with high density aluminium foam, after the dynamic compression.

The graphs showing and comparing the selected specimens of each configuration investigated under dynamic load are presented in Fig. 14. Figure 14 clearly reveals the highest compression force of the Foam\_B-filled specimen and its better energy absorbing parameters and overall performance. In the case of two other configurations compared to the empty tubes, energy absorbing parameters slightly increased and overall graph shapes slightly changed. Core materials caused reduction of a compression distance, as all the tests were evaluated with the same impact velocity and drop weight mass applied.

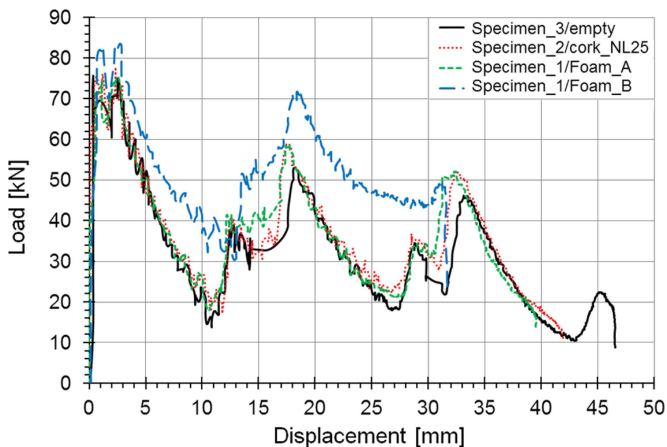


FIG. 14. Comparison of dynamic compression results for evaluating filling configurations.

As a measurement of the overall performance of the studied energy absorbing structures the absorbed energy per unit volume was introduced (Table 3). It was calculated as the ratio of absorbed energy to volume of the crashed part of the specimen. To compare the configurations, the volume structural efficiency parameter was obtained. For the empty tubes, this parameter is equal to 1, as the corresponding value is divided by itself. Other modified configurations should have this parameter as high as possible. In the case of Foam\_A and Cork\_NL25, volume structural efficiency was higher by about 14–15% (Table 3). Foam\_B configuration achieved a much higher result equal to 1.59. This structure has higher crushing load efficiency. A drawback of this structure is very low stroke efficiency (US).

The compression stress-strain curves of the investigated square-section samples of the core materials are presented in Fig. 15. In the case of Foam\_A and Cork\_NL25, a force level in the middle part of their curves is very low compared to Foam\_B. Table 4 presents characteristic dimensions and results for the performed tests of the core materials. Mean crushing stress (MCS) referenced to the initial cross-section area, US and SE were obtained and calculated.

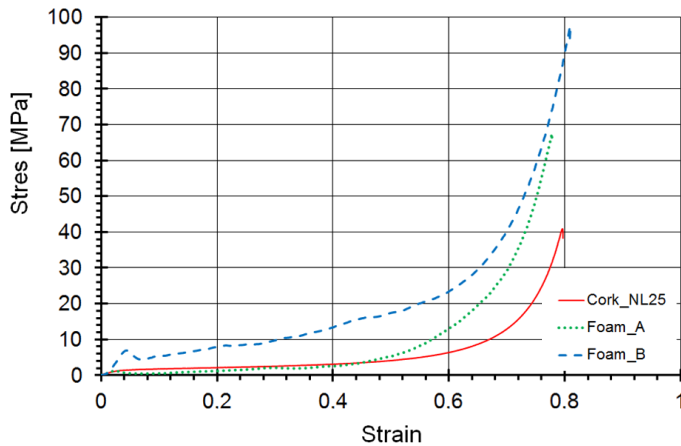


FIG. 15. Static compression graph for the filling materials.

**Table 4.** Dimensions and results for static tests of filling materials.

Filling	Dimensions [mm]	Height [mm]	Mean crushing stress [MPa]	Useful stroke [mm]	Stroke efficiency
Cork_NL25	50 × 50	50	2.53	25.1	0.50
Foam_A	50 × 50	26	1.98	11.6	0.45
Foam_B	50 × 50	26	10.12	15.4	0.59

WIERZBICKI *et al.* [14–16] and HANSEN *et al.* [3, 6] suggested an empirical formula for the crushing resistance of the square foam-filled columns. Both methods used the following representation for MCF [14]:

$$(3.1) \quad P_{m,f} = P_m + \Delta P,$$

where  $P_{m,f}$  and  $P_m$  are characteristic loads of filled and empty column respectively, and

$$(3.2) \quad \Delta P = C_I f(\sigma_0, \sigma_f, \xi).$$

$C_I$  represents the strengthening constant and  $f(\sigma_0, \sigma_f, \xi)$  is an interaction function determined from the dimensional analysis to capture the strengthening mechanism. Parameters  $\sigma_0$ ,  $\sigma_f$  are plastic flow stress of the column material and the crushing strength of the foam filler, respectively, and  $\xi$  is a geometrical parameter. For a square box column with a cross section  $b \times b$ , SANTOSA and WIERZBICKI'S [14, 15] prediction of the MCF increase for the foam-filled column was proposed as:

$$(3.3) \quad \Delta P = 2b^2 \sigma'_f,$$

where  $\sigma'_f$  specifically means crushing strength of foam.

HANSEN *et al.* [6] proposed that in the case of axial compression, the strengthening interaction  $\Delta P$  can be divided into two different components, which are the direct uniaxial compressive strength of the foam  $\Delta P_1$  and the wall-foam strengthening mechanism  $\Delta P_2$ . In this variant, the strengthening interaction  $\Delta P$  is equal to

$$(3.4) \quad \Delta P = \Delta P_1 + \Delta P_2 = 2b^2 \sigma_f + 5bt \sqrt{\sigma_f \sigma_0}.$$

Hansen defines  $\sigma_f$  as a foam plateau stress and  $\sigma_0$  as an arithmetic average from extrusion plastic stress and ultimate stress.

Both Eqs. (3.3) and (3.4) are dedicated to column profiles of square section  $b \times b$  and wall thickness  $t$ . Due to the round shape of the specimens studied in this paper, these equations cannot be used directly. HANSEN *et al.* [4, 5] developed, using the same procedure, an additive design formula for determination of the interaction effect of circle foam-filled extrusions. Hence,  $\Delta P$  is modelled as [4]

$$(3.5) \quad \Delta P = \frac{\pi}{4} \sigma_f (b - 2t)^2 + C \sigma_f^\alpha \sigma_0^{(1-\alpha)} (b - t)^\beta t^{(2-\beta)},$$

where  $C$ ,  $\alpha$  and  $\beta$  are dimensionless constants, whereas  $b$  and  $t$  are the outer diameter and wall thickness of the extrusion, respectively. In Eq. (3.5),  $\sigma_f$  is defined as a foam plateau stress, expression  $(\pi/4) \sigma_f (b - 2t)^2$  is the uniaxial

resistance of the foam filler and the last term describes the interaction effect. To express the interaction effect, the dimensionless parameters  $C$ ,  $\alpha$  and  $\beta$  were chosen by the authors, based on the conducted experimental results and appropriate FEM simulations, in the way that the error between model and experiments is minimised [4]. The obtained optimum values for  $\alpha$  and  $\beta$  were very close to the corresponding values for square section aluminium extrusion applied in [6], being 0.5 and 1.0, regardless of applying the characteristic stress  $\sigma_0$  or the energy equivalent flow stress to represent the behaviour of the extrusion material. For this reason, in the current analyses constants  $\alpha$  and  $\beta$  were fixed as 0.5 and 1.0. As presented in [4],  $C$  is an increasing function of deformation, and, moreover, this function is linear. After applying fixed  $\alpha$  and  $\beta$  Eq. (3.5) can be written as

$$(3.6) \quad \Delta P = \frac{\pi}{4} \sigma_f (b - 2t)^2 + C \sqrt{\sigma_f \sigma_0} (b - t) t.$$

The final formula describing the total crushing force of the core-filled round columns has the following form:

$$(3.7) \quad P_{m,f} = P_m + \Delta P = P_m + \frac{\pi}{4} \sigma_f (b - 2t)^2 + C \sqrt{\sigma_f \sigma_0} (b - t) t.$$

Based on the above equation, constants  $C$  were calculated for all three investigated core types. The presented values correspond to maximum strokes from the dynamic tests, which were around 30–40% of the total length (see Table 2). This is approximately a half of the useful stroke values, therefore  $C$  can be treated as an average value of this parameter, which generally is a linear function of specimen shortening [4]. Moreover, this parameter represents proportionality between wall-foam strengthening mechanism contribution to increase of crushing force, core and extrusion strength, and dimension parameters. The higher the value the better interaction between tube and filler, even despite lower core and extrusion strength.

The analysis of the crushing force increase components  $\Delta P_1$ ,  $\Delta P_2$  and constant  $C$  is presented in Table 5.  $P_m$  in Eq. (3.7) is MCF of the empty tubes and is equal to 28.7 kN on average (Table 2). Experimental MCF increase  $\Delta P$  is based on difference between  $P_{m,f}$  and  $P_m$ . Stress  $\sigma_f$  is the average stress from the plateau of core compression curves (Fig. 5), given in Table 4 as the MCS of the core. Tube characteristic stress  $\sigma_0 = 187.5$  MPa is an arithmetic average from the plastic stress 160 MPa and ultimate stress 215 MPa for aluminium 6060 T66 alloy.

The crushing force increase resulting from the direct uniaxial compressive strength of the foam was obtained as  $\Delta P_1$  based on equation:

$$(3.8) \quad \Delta P_1 = \frac{\pi}{4} \sigma_f (b - 2t)^2.$$

**Table 5.** Analysis of the crushing force increase components.

Filling	Experimental MCF increase $\Delta P$ [kN]	Increase from the uniaxial compressive strength $\Delta P_1$ [kN]	Increase from wall-foam strengthening mechanism $\Delta P_2$ [kN]	Wall-foam strengthening mechanism share $R_{\Delta P_2}$ [%]	Stroke $D_{\max}$ [%]	Constant $C(D_{\max})$
Cork_NL25	5.2	4.2	1.0	19.1	0.42	0.48
Foam_A	3.8	3.3	0.5	13.4	0.40	0.28
Foam_B	18.9	16.8	2.1	11.0	0.33	0.50

Dimensions of the tubes are as follows (Table 1): outer diameter  $b = 50$  mm and thickness of the wall  $t = 2$  mm. Wall-foam strengthening mechanism share  $R_{\Delta P_2}$  represents the percentage share of the second part of the force increase in  $\Delta P$ , resulting from wall-foam crushing mechanism, and it is calculated as follows:

$$(3.9) \quad R_{\Delta P_2} = \frac{\Delta P_2}{\Delta P} 100\% = \frac{\Delta P - \Delta P_1}{\Delta P} 100\%.$$

As shown in Table 5, Foam\_B has the highest overall  $\Delta P$  increase of 18.9 kN. This configuration has the best volume structural efficiency (Table 3) and it has also the highest value of constant  $C$  representing proportionality between core and tube dimensional and strength parameters and  $\Delta P_2$ .  $C$  is equal to 0.5.  $\Delta P_2$  share in  $\Delta P$  is the lowest – 11%, which means that crushing force increased mainly due to foam strength itself. Despite very low MCF increase, about 5 kN, Cork\_NL25 has shown  $C$  value similar to Foam\_B and also the highest  $R_{\Delta P_2}$ . Almost 20% of the force increase was due to wall-foam interaction, thus, according to these criteria, Cork\_NL25 showed the best properties.

Foam\_A seems to be the worst material in almost every aspect of the parameters defining energy absorbing capabilities. It showed the lowest force increase, wall-foam strengthening mechanism share and the lowest  $C$ .  $V/E$  was also very low.

#### 4. CONCLUSIONS

Conclusions drawn from the presented study of aluminium profiles filled with different materials are as follows:

- 1) Foam\_A and Cork\_NL25 fillings had a limited impact on the crushing charts. Energy absorbing properties are only slightly higher compared to the data of the empty samples. The level of the crushing force, which was observed in static compression tests conducted separately for Cork\_NL25

and Foam\_A, is low. Volume structural efficiency for Foam\_A- and Cork\_NL25- filled tubes increased by about 14–15%.

- 2) In the case of profiles filled with Foam\_B, there is a visible increase in crushing force compared to the empty samples. Energy absorbing parameters are also high compared to the other filled configurations, except for the useful stroke and stroke efficiency. Volume structural efficiency achieved a much higher result equal to 1.59.
- 3) Despite very low MCF increase, Cork\_NL25 has shown the highest  $R_{\Delta P_2}$ . Almost 20% of the force increase was due to wall-foam interaction, therefore, according to these criteria, Cork\_NL25 showed the best properties.  $C$  value is similar to that in the Foam\_B specimen.
- 4) Cylinders were crushed with axisymmetric buckling, while foam cores were crushed plastically in a diamond buckling mode. The graphs of force of all the compared filling configurations are saw-like shaped. Each “tooth” corresponds to the folding of the aluminium profile.
- 5) Cork material during the crush worked in its elastic range. After the test, the cork inserts returned almost to their initial height. Plastic deformation also occurred. However, it did not represent a significant share in overall cork deformation.

This paper presented the study of aluminium profiles filled with cork and compared them to fillings of foam materials and unfilled samples.

#### ACKNOWLEDGMENT

The work has been accomplished under the research project: DOBR-BIO4/022/13149/2013 financed by the National Centre of Research and Development (NCBiR).

#### REFERENCES

1. ALEM N.M., STRAWN G.D., *Evaluation of an energy-absorbing truck seat for increased protection from landmine blasts*, USAARL Report No. 96-06, U.S. Army Aeromedical Research Laboratory, Fort Rucker, Alabama, 1996.
2. ALGHAMDI A.A.A., *Collapsible impact energy absorbers: an overview*, Thin-Walled Structures, **39**(2): 189–213, 2001.
3. HANSEN A.G., LANGSETH M., *Development in aluminium based crash absorption components*, Presented to the Norwegian-French Industry Conference in Paris, November 1996, The Norwegian University of Science and Technology, N-7034 Trondheim, Norway, 1996.
4. HANSEN A.G., LANGSETH M., HOPPERSTAD O.S., *Static and dynamic crushing of circular aluminium extrusions with aluminium foam filler*, International Journal of Impact Engineering, **24**(5): 475–507, 2000.

5. HANSEN A.G., LANGSETH M., HOPPERSTAD O.S., *Static and dynamic crushing of square aluminium extrusions with aluminium foam filler*, International Journal of Impact Engineering, **24**(4): 347–383, 2000.
6. HANSEN A.G., LANGSETH M., HOPPERSTAD O.S., *Static crushing of square aluminium extrusions with aluminium foam filler*, International Journal of Mechanical Sciences, **41**(8): 967–993, 1999.
7. HARTE A.M., FLECK N.A., ASHBY M.F., *Energy absorption of foam-filled circular tubes with braided composite walls*, European Journal of Mechanics – A/Solids, **19**: 31–50, 2000.
8. KECMAN D., *An engineering approach to crashworthiness of thin-walled beams and joints in vehicle structures*, Thin-Walled Structures, **28**(3/4): 309–320, 1997.
9. KELLAS S., JONES L.E., *Energy absorbing seat system for an agricultural aircraft*, NASA/CR-2002-212132, December 2002.
10. KREMER K., *Metal foams for improved crash energy absorption in passenger equipment*, Final Report for High-Speed Rail IDEA Project 34, Fraunhofer USA, Newark, Delaware, 2004.
11. MAYVILLE R.A., JOHNSON K.N., STRINGFELLOW R.G., TYRELL D.C., *The development of a rail passenger coach car crush zone*, Proceedings of the 2003 IEEE/ASME Joint Rail Conference, Chicago, Illinois, 2003.
12. NIU M.C.Y., *Composite airframe structures: practical design information and data*, Con-milit Press Ltd, Hong Kong 1992.
13. PEREIRA M.S., *Structural crashworthiness of railway vehicles*, Proceedings of the 5th World Congress of Rail Research, Montreal, Canada, 2006.
14. SANTOSA S.P., WIERZBICKI T., HANSEN A.G., LANGSETH M., *Experimental and numerical studies of foam-filled sections*, International Journal of Impact Engineering, **24**(5): 509–534, 1999.
15. SANTOSA S., WIERZBICKI T., *Crash behavior of box column filled with aluminum honeycomb or foam*, Computers & Structures, **68**(4): 343–367, 1998.
16. SANTOSA S., WIERZBICKI T., *Effect of an ultralight metal filler on the bending collapse behavior of thin-walled prismatic columns*, International Journal of Mechanical Sciences, **41**: 995–1019, 2000.
17. TABIEI A., NILAKANTAN G., *Reduction of acceleration induced injuries from mine blasts under infantry vehicles*, 6th European LS-DYNA Users Conference, Gothenburg, Sweden, 2007.
18. TYRELL D., TSAI T., *Improved crashworthiness of rail passenger equipment in the united states*, World Congress on Railway Research, Montreal, Canada, June, 2006.
19. UBELS L.C., WIGGENRAAD J.F.M., *Increasing the survivability of helicopter accidents over water*, National Aerospace Laboratory, NLR-TP-2002-110, February 2002.

*Received December 20, 2016; accepted version July 19, 2017.*

---